Biogenesis of the Secretory Granule: Chromogranin A Coiled-Coil Structure Results in Unusual Physical Properties and Suggests a Mechanism for Granule Core Condensation†

Coleman A. Mosley,‡,§ Laurent Taupenot,*,‡,|| Nilima Biswas,‡,|| Joseph P. Taulane,⊥ Norman H. Olson,⊥ Sucheta M. Vaingankar,|| Gen Wen,|| Nicholas J. Schork,# Michael G. Ziegler,|| Sushil K. Mahata,*,||,#,○ and Daniel T. O'Connor*,||,#,▽,○

Bioinformatics Graduate Program, Departments of Medicine, Chemistry, and Pharmacology, and Center for Human Genetics and Genomics, University of California at San Diego, and VA San Diego Healthcare System, San Diego, California

Received April 14, 2007; Revised Manuscript Received June 23, 2007

ABSTRACT: The secretory pro-hormone chromogranin A (CHGA) is densely packed into storage granules along with catecholamines, playing a catalytic role in granule biogenesis. 3-Dimensional structural data on CHGA are lacking. We found a superfamily structural homology for CHGA in the tropomyosin family of alpha-helical coiled-coils, even in mid-molecule regions where primary sequence identity is only modest. The assignment was confirmed by an independent algorithm, suggesting ∼6−7 such domains spanning CHGA. We provide additional physiochemical evidence (chromatographic, spectral, microscopic) consistent with this unusual structure. Alpha-helical secondary structure (at up to ∼45%) was confirmed by circular dichroism. CHGA molecular mass was estimated by MALDI-TOF mass spectrometry at ∼50 kDa and by denaturing gel filtration at ∼50−61 kDa, while its native Stokes radius was ∼84.8 Å, as compared to an expected ∼30 Å; the increase gave rise to an apparent native molecular weight of ∼578 kDa, also consistent with the extended conformation of a coiled-coil. Small-angle X-ray scattering (SAXS) on CHGA in solution best fit an elongated cylindrical conformation in the monodisperse region with a radius of gyration of the rod cross-section (R_t) of ∼52 Å, compatible with a coiled-coil in the hydrated, aqueous state, or a multimeric coiled-coil. Electron microscopy with negative staining revealed an extended, filamentous CHGA structure with a diameter of ∼94 ± 4.5 Å. Extended, coiled-coil conformation is likely to permit protein "packing" in the secretory granule at ∼50% higher density than a globular/spherical conformation. Natural allelic variation in the catestatin region was predicted to disrupt the coiled-coil. Chromaffin granule ultrastructure revealed a ∼108 ± 6.3 Å periodicity of electron density, suggesting nucleation of a binding complex by the CHGA core. Inhibition of CHGA expression, by siRNA, disrupted regulated secretory protein traffic by ∼65%, while targeted ablation of the CHGA gene in the mouse reduced chromaffin granule cotransmitter concentrations by ∼40−80%. These results suggest new roles for secretory protein tertiary structure in hormone and transmitter storage, with implications for secretory cargo condensation (or dense core "packing" structure) within the regulated pathway.

CHGA[1] is the first discovered of the "granin" pro-hormone series mediating catecholamine storage and release (*1*). The primary amino acid sequence (*2*, *3*) extensive genomic sequencing of polymorphic alleles (*4*) and phenotypic expression of CHGA in hypertension (*5*) have been well documented, but its 3-dimensional structure is not known. The NMR structure of the active catestatin fragment of CHGA (human $CHGA_{352-372}$) has been solved and deposited at the Protein Data Bank (*6*), but there remain questions about the physical properties of the entire 439 amino acid mature human pro-hormone, and mechanisms for its known extremely dense packing within secretory granules (at up to ∼200 mg/mL, or ∼4 mM (*7*−*9*). The complete human CHGA pre-pro-protein has an 18 amino acid signal peptide, a vasostatin (vasodilatory) domain immediately thereafter, and a series of biologically active peptides, including the catecholamine release-inhibitory catestatin, human $CHGA_{352-372}$ (*6*), bounded by a dibasic cleavage site at the carboxy-terminus.

† The work was supported by the Department of Veterans Affairs, National Institutes of Health, and Bioinformatics Program, UCSD. The Stanford Synchrotron Radiation Laboratory (SSRL) is a national user facility operated by Stanford University on behalf of the U.S. Department of Energy, Office of Basic Energy Sciences. The SSRL Structural Molecular Biology Program is supported by the Department of Energy, Office of Biological and Environmental Research, and by the National Institutes of Health, National Center for Research Resources, Biomedical Technology Program. The UCSD Cryo-Electron Microscopy Facility is supported by NIH Grants 1S10RR20016 and GM033050 to Dr. Timothy S. Baker and a gift from the Agouron Institute to UCSD.

* Correspondence to these authors: Department of Medicine (0838), UCSD School of Medicine, 9500 Gilman Drive, La Jolla, CA 92093-0838. Tel: (858)-5340661. Fax: (858)-5340626. E-mail: doconnor@ucsd.edu, ltaupenot@ucsd.edu, or smahata@ucsd.edu.

‡ These authors contributed equivalently to the work.

§ Bioinformatics Graduate Program, University of California at San Diego.

|| Department of Medicine, University of California at San Diego.

⊥ Department of Chemistry, University of California at San Diego.

Center for Human Genetics and Genomics, University of California at San Diego.

▽ Department of Pharmacology, University of California at San Diego.

○ VA San Diego Healthcare System.

[1] Abbreviations: CD, circular dichroism; CHGA, chromogranin A; EOL, Encyclopedia of Life project; MALDI-TOF, matrix-assisted laser desorption ionization/time-of-flight mass spectrometry; M_{app}, apparent molecular weight (kDa; by interpolation between standards on gel filtration); R_S, Stokes radius (Å); SAXS, small-angle X-ray scattering; SDS, sodium dodecyl sulfate.

10.1021/bi700704r CCC: $37.00
Published on Web 08/24/2007

The rapid proliferation of genomic sequencing has outpaced the capacity to experimentally establish the 3-dimensional structures of proteins. Indeed, up to 55 different polymorphic variants are now known within human CHGA itself (*4*). Many methods for protein fold predictions exist (*10*), but there is no consensus on optimal prediction methods. For example, entire proteomes have been matched to a set of known 2- and 3-dimensional templates derived from the Protein Data Bank (PDB) and the Structural Classification of Proteins (SCOP) by a set of *in silico* methods to assign putative folds (*11*, *12*). The growing gap between proteome-scale sequence data and proven structural data engenders a need for reliable *in silico* methodology for structural analysis. Even with extensive biochemical data on CHGA, the lack of structural knowledge impedes further refinement of the mechanisms of action for this important class of pro-hormone in human disease.

CHGA has highly unusual physical properties, with elution from gel filtration media suggesting an effective molecular (Stokes) radius (R_S) far higher than that predicted by its molecular mass at ~49 kDa (*13*). CHGA can exist as a homodimer (*14*) and perhaps even a homotetramer, with a consequent increase in apparent molecular weight (*15*). However no prior experiment has produced a model that explains all of these peculiar physical properties.

Multiple species' CHGA and its several known human genetic variants (*4*) formed the queries for a protein annotation pipeline (*11*), to assess its likely structure. The goal was to combine the known physical properties with the predicted 3-dimensional structure, and form hypotheses about their relationships. Our initial homology results, followed by extensive confirmation with several experimental techniques (chromatographic, spectral, and microscopic), suggest a novel higher order structure for CHGA of the coiled-coil variety, which may explain several of the unique physical properties of the protein, with potential implications for the biogenesis of the endocrine secretory vesicle.

EXPERIMENTAL PROCEDURES

CHGA Primary Structure and Sequence Variants. Common amino acid replacement sequence variants in CHGA were discovered by systematic resequencing of each of the eight *CHGA* exons, in genomic DNA from $n = 180$ individuals ($2n = 360$ chromosomes), as previously described (*4*).

Homology Modeling. Twelve naturally occurring amino acid replacement variants (*4*) of human CHGA (initially wild-type, plus the catestatin variants Gly364Ser, Pro370Leu, and Arg374Gln; subsequently Glu71Gly, Glu158Lys, Glu246Asp, Arg253Trp, Ala256Gly, Leu314Pro, Gly297Ser, and Arg381Trp) were processed via the "123D" algorithm within the EOL "pipeline" against its template of folds (FOLDLIB, <http://foldlib.sdsc.edu>) derived from both the PDB (Protein Data Bank, <http://www.rcsb.org/pdb>) and SCOP (Structural Classification of Proteins, <http://scop.mrc-lmb.cam.ac.uk/scop/>) (*11*, *12*, *16*). The CHGA alignment was fitted to the mature protein (i.e., the initial 18 amino acid hydrophobic signal peptide of the pre-hormone was not included, since this segment of the protein is cleaved cotranslationally). This pipeline performs a sequence homology search via BLAST (Basic Local Alignment Search Tool) and an iterative sequence homology search via PSI-BLAST (Position Specific Iterative BLAST) (*17*) <http://helix.nih.gov/docs/gcg/psiblast.html> using 3 iterations and a cutoff *e*-value of $<10^{-6}$. The threading and "contact capacity" program "123D" <http://123d.ncifcrf.gov/123D+.html> sequentially aligns sequences to known templates (the EOL fold library derived from SCOP and PDB), by recursively partitioning and subdividing the query sequence so as to optimize the 3-D match (the "contact capacity" between query and object), restricting domains to >30 amino acids in length; the algorithm uses PSI-BLAST output profiles as its initial input, providing the top 50 matches with their assigned *z*-scores (*18*) (*19*). Structures resulting from these algorithms compare favorably to those obtained from other homology modeling procedures (*16*, *19*). Gapped BLAST and PSI-BLAST use "affine gap costs" which charge the score $-a$ for the existence of a gap, and the score $-b$ for each residue in the gap. Thus a gap of k residues receives a total score of $-(a + bk)$; specifically, a gap of length 1 receives the score $-(a + b)$ (*17*) <http://www.ncbi.nlm.nih.gov/BLAST/matrix_info.html#matrix>.

Previously the entire human proteome was processed through the EOL pipeline (*12*), and species-specific "benchmarking" (see below) of all three methods was performed (*16*). The "benchmarking" assignment "accuracy" is defined for a given *e* (expectation)-value or *z*-score interval as the number of true positive fold predictions divided by the number of true and false positive fold predictions for this species against the entire fold library. A true positive is defined as a consistent fold assignment, while a false positive is defined as an ambiguous or inconsistent assignment. These "benchmark" standards were used to assign a reliability to the CHGA homology output, with "A" reliability representing ≥99.9% accuracy in fold assignment, "B" reliability at 99.0−99.9% accuracy, and "C" reliability at 90.0−99.0% accuracy (*20*).

The alignment provided the structural template for energy mimimization by molecular dynamics with spatial restraints in Modeller version 7 (*21*) <http://salilab.org/modeler/modeler.html>.

Secondary Structure Modeling/Predictions

Simple secondary structure predictions (alpha-helix, strand [beta-sheet], loop) were accomplished by a neural network method (*22*, *23*) using the on-line PredictProtein web-server <http://www.predictprotein.org/results/bh5953gx.html>. These predictions included solvent accessibility (core/surface [*e*/*b*] ratio).

Coiled-coil predictions were accomplished by using the on-line COILS web-server <http://www.ch.embnet.org/software/COILS_form.html>, searching for regions that are strongly amphipathic, displaying a pattern of alternating hydrophilic and hydrophobic residues that is repeated every 7 residues (heptad repeat residues a → g, with a and d hydrophobic) as outlined by Lupas et al. (*24*).

Physical Properties of CHGA

Gel Filtration in Native and Denatured Conditions. Native CHGA was purified from freshly isolated chromaffin granules of bovine adrenal medulla and human pheochromocytoma as previously described (*25*−*27*). Homogeneity was verified by SDS−PAGE, and amino-terminal sequencing (*28*).

The Stokes (effective molecular) radius (R_S) of CHGA under native conditions was established by gel filtration on a 50 × 0.75 cm TSK-4000 SW column, run at 1 mL/min in 0.2 M Na phosphate buffer, pH = 6.5. Size standards (Amersham) on this column were as follows: *a* (thyroglobulin, 669 kDa, 86 Å), *b* (ferritin, 440 kDa, 79 Å), *c* (gamma globulin, 160 kDa, 55.5 Å), *d* (catalase, 232 kDa, 52 Å), *e* (bovine serum albumin dimer, 132 kDa, 43.5 Å), *f* (bovine serum albumin monomer, 66 kDa, 35.5 Å), *g* (ovalbumin, 45 kDa, 27.3 Å), and *h* (lysozyme, 14.3 kDa, 20 Å). Elution was expressed as $(-\log_{10} K_d)^{1/2}$, where $K_d = (V_t - V_e)/V_t$, V_e = elution volume, and V_t = total internal volume. Stokes radius (R_S, in Å) was estimated by interpolation on the standard Laurent−Killander plot of R_S versus $(-\log_{10} K_d)^{1/2}$. Apparent molecular weight (M_{app}, in kDa) was also determined by interpolation on the plot of M_{app} versus $(-\log_{10} K_d)^{1/2}$.

The molecular weight of CHGA, under denaturing conditions (*29*, *30*) was estimated by gel filtration on the same column, at 0.8−1.0 mL/min elution, but with the following buffers: 6 M guanidine HCl, 0.05 M Na phosphate, pH = 6.5; or 0.1% (w/v) SDS, 0.05 M Na phosphate, pH = 6.5.

Recombinant Wild-Type Human CHGA. The human CHGA cDNA was resequenced to verify wild-type bases and encoded amino acids at each position (*4*), and then recombinant human CHGA was expressed and purified as previously described, using a terminal 6-His-affinity-tag (*31*). After affinity isolation, the purity of recombinant human CHGA was characterized by three techniques: SDS−PAGE; amino-terminal amino acid sequencing (6 cycles) on 50 pmol of purified protein using an Applied Biosystems PROCISE 494HT Protein Sequenator <http://proteinsequencer.ucsd.edu/>; and MALDI-TOF (matrix-assisted laser desorption ionization/time-of-flight) mass spectrometry. Five picomoles of recombinant human CHGA was analyzed on a PE Biosystems Voyager DeSTR MALDI-TOF mass spectrometer with a nitrogen laser, operating in a linear mode using sinapinic (3,5-dimethoxy-4-hydroxycinnamic) acid as matrix <http://chem-tech.ucsd.edu/Recharges/MassSpec/equip-biomol.html>.

Circular Dichroism for Secondary Structure. The molar ellipticity ([θ], deg·cm^2/dmol) of recombinant human CHGA (wild-type amino acids) was determined at 25 °C with the protein at 300 μg/mL (∼5 μM) in 10 mM Na phosphate buffer, pH 5.2, or 10 mM Tris, pH 7.4; some CD experiments were conducted in 50% 2,2,2-trifluoroethanol (TFE). Other CD experiments were conducted in higher salt concentration, either 0.5 or 1.0 M NaF (to minimize spectral noise in the far UV). Spectra were collected over 190−260 nm in a Aviv model 215 circular dichroism spectrometer (Aviv Biomedical, Lakewood, NJ <http://www.avivbiomedical.com/>) with a 0.2 cm path length (*32*), collecting data at 0.5 nm intervals. Two repeat scans were obtained for each sample, and a baseline spectrum was subtracted from the average. From the ellipticity data, % contributions of alpha-helix, strand/beta-sheet, and random coil were computed (http://www.embl-heidelberg.de/∼andrade/k2d/) using the neural network algorithm "K2d" trained on 18 protein templates (*33*, *34*).

Small-Angle X-ray Scattering (SAXS). SAXS of recombinant wild-type human CHGA was conducted on beamline 4-2 at the Stanford Synchrotron Research Laboratory (SSRL <http://www-ssrl.slac.stanford.edu/∼saxs/>), as previously described for other proteins in aqueous solution (*35*, *36*). CHGA was studied at 5−20 mg/mL (∼0.1−0.4 mM) in aqueous solution buffered by either 1 mM Tris pH = 7.0 or 1 mM MES pH = 5.5 (i.e., intragranular pH), in the presence or absence of $CaCl_2$ at 10 mM. Just prior to SAXS, protein solutions were centrifuged at ∼13,000 RPM for 30 s, to remove macroscopic aggregates. Results of SAXS were analyzed and plotted as described (*37*, *38*).

Electron Microscopy of CHGA. Recombinant human CHGA (at 20 mg/mL) was placed on glow-discharged, carbon support films and stained with 1% aqueous uranyl acetate. The grid was examined and images recorded with a FEI Tecnai G2 Sphera electron microscope at 200kV <http://cryoem.ucsd.edu/>. Negatively stained protein fibers were then observed.

Transmission Electron Microscopy of Chromaffin Granules. Human chromaffin granules were prepared from a fresh homogenate of human pheochromocytoma sedimented on a 0.6 M/1.6 M sucrose density step gradient, as previously described (*25*, *26*) <http://medicine.ucsd.edu/hypertension/protocols.htm>. Purified granules were visualized on transmission electron microscopy after fixation with osmium tetroxide and dual staining with lead citrate and uranyl acetate, as previously described (*25*, *26*). Morphometry was conducted by replicate (n = 5) measurements over an 8 × 10 in. image at a magnification of 135,000 diameters.

Role of CHGA in the Chromaffin Cell Regulated Secretory Pathway: Transmitter Exocytosis

Cell Culture and Silencing of CHGA Expression by siRNA. PC12 rat pheochromocytoma cells were cultured as previously described (*39*). Two days before transfection, cells were split onto poly-L-lysine (Sigma) coated 12-well Costar plates. Pools of ∼22 bp siRNA duplexes targeting an 800 bp coding region of rat CHGA or a 700 bp domain green fluorescent protein (GFP) gene (as a control for specificity) were prepared using a dicer siRNA generation kit (Genlantis) according to the manufacturer's protocol. PC12 cells were transfected with 0−4 μg/well of a pool of siRNAs, using GeneSilencer transfection reagent (Genlantis) according to the manufacturer's instructions. In cotransfection experiments 1.25 μg/well of the expression plasmid for human growth hormone (pXGH5, Nichols Institute) was added to siRNAs. Twenty-four hours after the beginning of the transfection, culture medium was replaced and cells were further cultured for 72−96 h. CHGA expression was evaluated by immunoblotting. Total cell lysates were prepared by detergent extraction for 20 min at 4 °C in a buffer containing 10 mM NaCl, 1% Triton X-100, 1 mM DTT, 5 mM EDTA, protease inhibitors cocktail (Calbiochem), 50 mM Tris-HCl pH 8.0. The lysate were cleared by centrifugation at 23000*g* for 10 min at 4 °C. Proteins were separated by SDS−PAGE on 10% polyacrylamide gels (NuPage, Invitrogen) and transferred onto nitrocellulose sheets (Schleicher and Schuell). Membranes were blocked for 1 h in buffer containing either 5% heat inactivated fetal calf serum (FCS) plus 0.05% Tween 20 in PBS, or in 5% nonfat dry milk in PBS (NFDM-PBS). Nitrocellulose blots were incubated for 2 h with either a rabbit polyclonal anti-catestatin (rat $Chga_{363-383}$; 1:1000 in 5% NFDM-PBS), or a mouse monoclonal anti-actin (I-19,

Table 1: Sequence Alignments to Tropomyosin: CHGA by Species[a]

CHGA species	initial BLAST alignment to mature human CHGA: amino acid alignment to human CHGA	initial BLAST alignment to mature human CHGA: identity score with human CHGA	EOL homology matching for CHGA: method for homology match	EOL homology matching for CHGA: homologue match to that species' CHGA	EOL homology matching for CHGA: aligned amino acids in that species' CHGA	EOL homology matching for CHGA: reliability score (fold assignment accuracy)
human	1−439 (self)	439 (self)	123D	tropomyosin 1c1g	48−349	B (99−99.9%)
pig	1−430	326	123D	tropomyosin 1c1g	54−334	A (≥99.9%)
horse	1−430	338	123D	tropomyosin 1c1g	54−348	A (≥99.9%)
bovine	1−431	316	123D	tropomyosin 1c1g	48−346	B (99−99.9%)
rat	1−412	241	123D	tropomyosin 1c1g	58−378	B (99−99.9%)
mouse	1−445	270	PSI-BLAST	meromyosin 1i84	57−346	C (90−99%)

[a] The BLAST and EOL outputs for the mature (after signal peptide excision) CHGA molecule from several species is shown. The human CHGA was the query for the BLAST results so the aligned amino acids of each target CHGA is shown and the number of identical amino acids. They are listed in decreasing homology compared to human. The EOL homology method is given for the match where each CHGA was the query protein against the EOL library of fold templates. There was only one match in this amino acid region for each CHGA protein at "C" or above reliability. The amino acids in the CHGA protein that aligned with the target are shown. Porcine (*Sus scrofa*) cardiac alpha-tropomyosin (TPM1; PDB ID 1c1g) is a 284 amino acid sequence. The alpha-helical portion of chicken (*Gallus gallus*) meromyosin (PDB ID li84) was matched to murine CHGA. The "reliability" score (A, B, C) is defined in the Experimental Procedures. PSI-BLAST (http://bioportal.weizmann.ac.il/education/materials/gcg/PSIBLAST.html): position-specific iterated BLAST (*17*, *74*).

Santa Cruz Biotechnology; 1:1000 in 5% FCS), and washed for 15 min with 0.05% Tween 20 in PBS. Blots were subsequently incubated for 1 h with a goat anti-mouse IgG conjugated to horseradish peroxidase (Biodesign International; 1:7500 in 5% FCS plus 0.05% Tween 20), or a goat anti-rabbit horseradish peroxidase conjugate (BioRad; 1:3000 in 5% NFDM-PBS). Immunoreactive bands were visualized by detection of peroxidase activity by chemiluminescence (Supersignal West Pico, Pierce). Protein expression was evaluated by densitometry (NIH image 1.6).

Regulated Exocytotic Secretion. PC12 cells transfected with an expression plasmid for human growth hormone GH (pXGH5, Nichols Institute) were grown on 12-well culture dishes. Cells were washed with calcium secretion buffer (CaSB: 150 mM NaCl, 5 mM KCl, 2 mM $CaCl_2$, 10 mM HEPES pH 7.4) and subsequently exposed to CaSB or to a barium containing secretion buffer (BaSB: 150 mM NaCl, 5 mM KCl, 2 mM $BaCl_2$, 10 mM HEPES pH 7.4) for 15 min. Supernatants were collected and cell lysates were prepared by quick freeze/thaw in CaSB containing 0.1% Triton X100. GH was measured in the culture supernatant and the cell lysate with colorimetric enzyme immunoassay (GH ELISA, Roche Diagnostics) using a Spectramax microplate reader. The secretion rate of GH is calculated as a percentage of total GH present in the cells before stimulation; total GH is the sum of the amount released plus the amount remaining in the cells.

Role of CHGA in the Chromaffin Cell Regulated Secretory Pathway: Cotransmitter Storage

Targeted ablation of the *Chga* locus in the mouse (homozygous *Chga*[−/−]) was accomplished and verified as previously described (*40*). The concentrations of multiple chromaffin granule cotransmitters were measured in adrenal gland homogenates of wild-type (+/+) versus homozygous knockout (−/−) mice, and expressed per adrenal gland: catecholamines, norepinephrine, and epinephrine, by radioenzymatic assay (*41*); neuropeptide Y (NPY), by enzyme immunoassay (Bachem AG); and ATP, by chemiluminescent assay (QuantiLum recombinant luciferase, Promega).

RESULTS

Homology Model: Coiled-Coil

Human CHGA had no extended homology matches via BLAST or PSI-BLAST against the library of fold templates, which simply indicates that complete/intact CHGA does not have a 3-D structure solved by X-ray crystallography or NMR in the PDB. However there was a structural match via the threading/contact capacity program 123D between an extended ∼302 amino acid stretch of the mid-molecule of human CHGA ($CHGA_{48-349}$) and the full length of porcine cardiac alpha-tropomyosin ($TPM1_{1-284}$) (*42*): an alpha-helical, coiled-coil protein with a solved X-ray crystal structure (PDB 1c1g). Within the human proteome (*12*), this match was specific at level "B" reliability, reflecting ∼99% accuracy for fold assignment as described in the Experimental Procedures. Intraspecific alignment of porcine tropomyosin to porcine CHGA (by 123D) yielded an "A" match (Table 1).

The human CHGA/tropomyosin alignment is shown in Supporting Information Figure I, spanning CHGA amino acids Ile_{48} through Asn_{349}. The homologous region spanned the entire length of a single tropomyosin chain ($TPM1_{1-284}$). The predicted CHGA coiled-coil terminates within the catestatin ($CHGA_{340-372}$) domain of CHGA, a region with known secondary (*43*) and tertiary structure (*44*) (*6*).

Supporting Information Figure II shows the predicted model of human $CHGA_{48-349}$ based on the 123D structural alignment with tropomyosin (TPM1). TPM1 structure 1c1g is a homotetramer, wherein the monomers ("A" and "B" chains) coil in a parallel manner within each coiled-coil homodimer, while two such homodimers align in antiparallel fashion to form the final homotetramer. Despite identical primary structures, the "A" and "B" chains of TPM1 do not have identical tertiary structures (*42*), since each alpha-helix bends as it spirals around its partner, with an approximate period of 7 residues per coiled turn (*24*).

Supporting Information Figure IIa displays human CHGA modeled to the tropomyosin "A" chain, and Supporting Information Figure IIb to the "B" chain: the near-complete coiled-coil homology of $CHGA_{48-349}$) is apparent in each

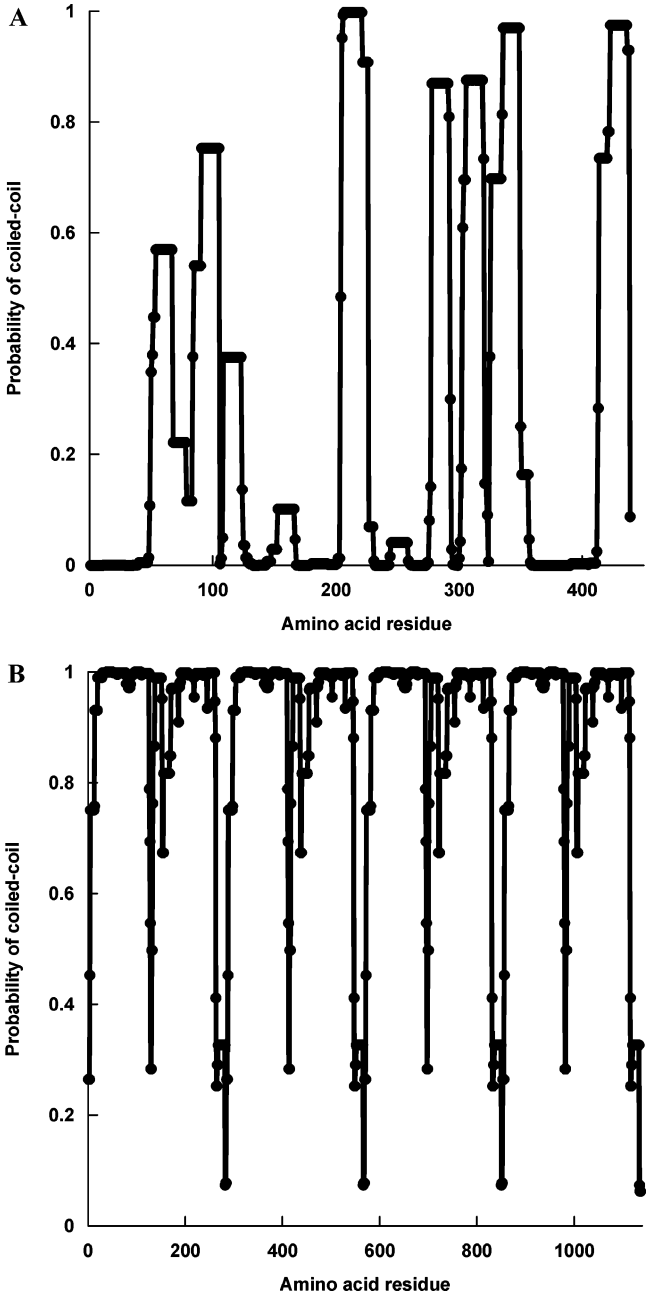

FIGURE 1: Predicted coiled-coil domains. The Coils algorithm <http://www.ch.embnet.org/software/COILS_form.html> searched for strongly amphipathic regions, displaying a pattern of alternating hydrophilic and hydrophobic residues repeated every 7 residues (heptad repeat residues a → g, with a and d hydrophobic). The minimum window was two such heptads, over 14 residues. The probability of coiled-coil structure is shown as a function of amino acid position. (A) Human CHGA (mature protein, after cleavage of signal peptide). (B) Porcine tropomyosin (TPM1).

case. The $CHGA_{48-349}$ homology to tropomyosin is disrupted by a single 19- to 29-amino acid nonaligned segment within CHGA: at $Val_{179}-Tyr_{197}$ in the "A" chain model (Figure 1a), and at $Ala_{174}-Lys_{202}$ in the "B" chain model (Supporting Information Figure IIb); in each case, the nonaligned region overlaps the biologically active chromacin peptide, $CHGA_{176-197}$, which may possess endogenous antimicrobial properties (*45*). This region of nonalignment (Supporting Information Figure II) might locally destabilize the coiled-coil, and perhaps enhance the susceptibility of the chromacin region to proteolytic excision from the CHGA pro-hormone.

Secondary Structure Predictions: Alpha-Helix and Coiled-Coil

The predicted (*22*, *23*) secondary structure across CHGA was 32.7% alpha-helix, 5.2% strand/beta-sheet, and 63.1% loop. The predicted residue accessibilities were 31.2% exposed: (surface >16%)/68.8% core (buried). Predicted (http://www.ch.embnet.org/software/COILS_form.html) coiled-coil domains in human CHGA (Figure 1a) revealed evidence for seven windows of ≥14 consecutive amino acids (i.e., ≥2 consecutive head-to-tail heptad amphiphilic repeats (*24*); probability >50%) in coiled-coil domains that spanned much of the molecule. Since CHGA may be phosphorylated on Ser/Thr residues (*46*), we probed the role charge by coiled-coil modeling on a CHGA template wherein we replaced each Ser or Thr by Asp, to mimic the effect of phosphorylation; the 7 CHGA regions predicted to have coiled-coil probability >50% were unaltered by this computational change in charge. Such Ser/Thr → Asp replacements might also serve to probe the effects of addition of anionic sugars to these residues during O-linked glycosylation (*46*).

In the adjacent panel of Figure 1b is a similar coiled-coil prediction for the known coiled-coil template, porcine tropomyosin (TPM1), showing an even greater propensity for coiled-coil domains across the molecule by the heptad repeat algorithm <http://www.ch.embnet.org/software/COILS_form.html>.

Physical Properties of Natural CHGA

Gel Filtration: Denaturing for Molecular Mass. Gel filtration under denaturing conditions (e.g., 6 M GuHCl or 0.1% SDS) can be used to estimate protein molecular weight by interpolation between known standard elutions (*29*, *30*), yielding a molecular weight estimation as a simple function of protein size, independent of conformation. The results of denaturing gel filtration of bovine and human CHGA demonstrate a molecular weight for human CHGA of ∼59 kDa in 6M GuHCl; and bovine CHGA at ∼61 kDa in GuHCl (Supporting Information Figure III-A) and ∼50 kDa in 0.1% SDS (Supporting Information Figure III-b). The findings are consistent with the primary structures of the mature proteins deduced from the cDNA sequences: 48,960 Da for human CHGA and 48,232 Da for bovine CHGA (*2*, *3*); somewhat higher values for actual (∼59−61 kDa) versus predicted (∼48−50 kDa) molecular weight are compatible with additional mass as a result of such post-translational modifications as glycosylation and phosphorylation (*46*, *47*).

Gel Filtration: Native Conformation for Stokes Radius. By contrast, native gel filtration demonstrated an effective Stokes radius (R_S) of ∼84.8 Å (Supporting Information Figure IV-A), yielding an apparent molecular weight of ∼578 kDa (Supporting Information Figure IV-B) for human CHGA. A globular protein of human CHGA's molecular weight (∼49 kDa) would have a predicted R_S ∼30 Å; the unexpectedly high R_S and apparent molecular weight suggest a highly asymmetric conformation compatible with the *in silico* findings of an extended coiled-coil (Table 1, Supporting Information Figure II).

Recombinant Wild-Type Human CHGA

Isolation and Characterization of Purity. After isolation by 6-His-tag affinity chromatography, recombinant CHGA

was homogeneous on SDS−PAGE, with an apparent molecular mass of ~65−70 kDa (Supporting Information Figure V left), consistent with previous reports (*25*); the discrepancy with the human CHGA mature protein's true molecular mass (at ~48,960 Da) may result from anomalous mobility in SDS−PAGE as a consequence of diminished SDS binding by the polyanionic CHGA (*48*). Indeed, by MALDI-TOF mass spectrometry (Supporting Information Figure V right), scanning across the entire *m*/*z* region from 10,000 to 200,000, the *m*/*z* of recombinant CHGA is 50,129, within experimental error (±300 Da) of the calculated mass of the recombinant protein (50,116 Da), taking into account the adventitious amino-terminal Met and the carboxy-terminal 6-His affinity tag. Amino-terminal sequencing of the recombinant protein over six residues yielded [Met]-Leu-Pro-Val-Asn-Ser, consistent with the known sequence of the mature CHGA protein (*48*), plus the adventitious amino-terminal Met residue. The minor MALDI-TOF peak at *m*/*z* 25,159 likely represents the +2 charge version of the 50,116 species.

Circular Dichroism for Secondary Structure. Circular dichroism (CD) has been used to follow the degree of alpha-helical and coiled-coil transition in tropomyosin, focusing on ellipticity minima in the 208 to 222 nm range to estimate this secondary structural feature (*32*, *49*). We studied the conformation of human CHGA by CD at two pH values, pH = 7.4 (neutral, extracellular) or pH = 5.2 (within the chromaffin granule), and finally at lower dielectric constant (in 50% trifluoroethanol [TFE]), to enhance the hydrophobic environment likely to occur at contact residues nucleating a coiled-coil. Human CHGA also demonstrated a CD spectrum with ellipticity minima at ~205 and ~222 nm, compatible with alpha-helical content (Figure 2): by K2d estimation (*33*, *34*), human CHGA secondary structural features were dependent upon solvent conditions, with the greatest display of alpha-helix at 45%, in the chromaffin granule pH = 5.2, with reduced dielectric constant (50% TFE). The especially deep ellipticity minima (Figure 2) are notable at pH = 5.2, in particular with TFE. The range of alpha-helical content found experimentally by CD for CHGA (28−45%, Figure 2) encompasses the predicted (*22*, *23*) value of 32.7%.

Although tropomyosin is known to be an alpha-helical coiled-coil on the basis of its X-ray diffraction structure (*50*), its alpha-helical content estimated by CD is highly dependent upon ionic strength, and most prominent at very high (~1−2 M) salt concentrations (*49*). Thus we also obtained the CHGA CD spectrum at higher ionic strength (0.5−1 M NaF, designed to minimize spectral noise at <200 nm (*32*)) at pH 5.2 and 7.4, in the absence of TFE; however, the ellipticity minima did not deepen with 0.5−1 M NaF, suggesting no further increase in alpha-helix, thus differing from the salt-dependence of the tropomyosin alpha-helix.

Small-Angle X-ray Scattering (SAXS) for Solution Shape. During SAXS, CHGA displayed a range of apparent self-association states (*37*, *38*), from monodisperse to polydisperse as judged by plots of either *I* (scattering intensity; Figure 3A) or *I***S* (intensity as a product of scattering angle; Figure 3C) as a function of Q^2 (sine of scattering angle).

To explore the likely shape of CHGA in this setting, we therefore chose measurements in the monodisperse regions of each spectrum (Figure 3B and 3D). Of note, the monodisperse region was the quantitatively most prominent feature of the spectrum, as judged by the histogram of scattering angle (1/*Q*; Figure 3E), suggesting that the monomeric form of CHGA predominates in solution.

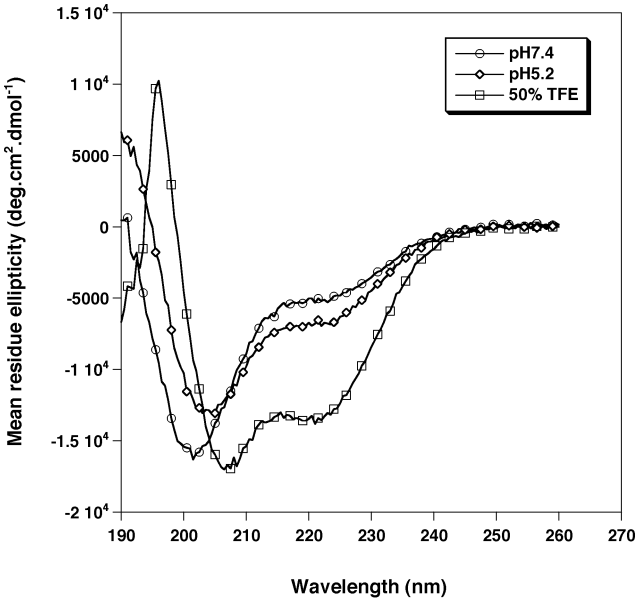

Condition	Value		
pH	7.4	5.2	5.2
Trifluoroethanol (TFE), %	-	-	50%
α-Helix, %	28%	31%	45%
ß-Sheet, %	17%	13%	23%
Random coil, %	55%	57%	31%

FIGURE 2: CHGA secondary structure probed by circular dichroism (CD). The CD spectrum of differential absorption of circularly polarized light was conducted in the far ultraviolet range (190−260 nm wavelength). Results are expressed as molar ellipticity ([θ], deg·cm^2/dmol). The spectra depict recombinant, purified human CHGA at 300 mg/L (~5 μM) in 10 mM Na phosphate, pH 5.2 (within the chromaffin granule core), or 10 mM Tris pH 7.4 (neutral, extracellular pH, after release from the cell). The effect of lowering the dielectric constant with 50% TFE (2,2,2-trifluoroethanol) is also shown. The CD spectra show local minima in the region of ~208 and ~222 nm, characteristic of alpha-helical content, estimated by the neural network algorithm "K2d" (see Experimental Procedures).

We then analyzed the monodisperse region scattering data (Q^2 = 0.04−0.06) using two models: the Guinier (sphere) relationship (Figure 3B) or a rod/cylinder model (Figure 3D). Clearly the rod model better fit the data than the sphere relationship, as judged either by visual inspection of the fit or by correlation coefficient (rod R = 0.999, versus sphere R = 0.879). We therefore fit the rod model to the scattering data, deriving a transverse radius of gyration of R_t = ~52 Å for the rod.

The continuously scaled self-association of CHGA (Figure 3A and 3C) occurred at either higher (~400 μM) or lower (~100 μM) CHGA concentration, and at either extracellular or intragranular pH (pH 7.0 or 5.5), even in the absence of macroscopic (visible) aggregation. When 10 mM $CaCl_2$ was added to the solution, followed by centrifugation at ~13,000 rpm (microfuge), the supernatant scattering intensity (*I* or *I***S*) at each scattering angle (Q^2) diminished markedly, suggesting macroscopic aggregation prior to spectroscopy, consistent with our previous observation that high calcium concentration aggregates CHGA (*51*).

Electron Microscopy (EM) of CHGA. After negative staining of CHGA adsorbed to the grid (Figure 4), *every* field examined displayed elongated filamentous structures that were quite atypical for the appearance of globular

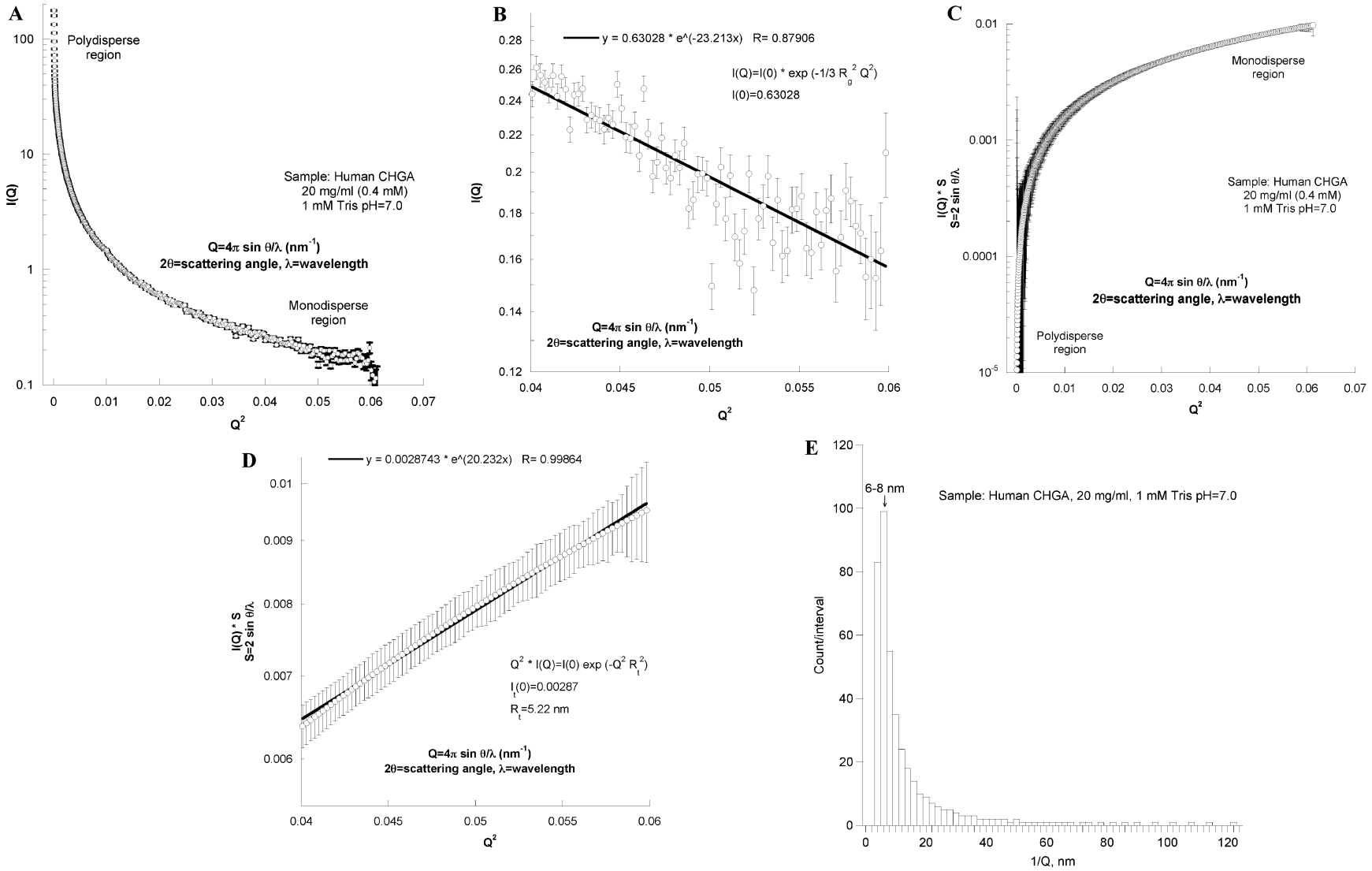

FIGURE 3: Small-angle X-ray scattering (SAXS) to probe CHGA conformation in solution. In the experiment pictured, recombinant human CHGA was studied at 20 mg/mL (∼400 μM) concentration at pH = 7.0 in 1 mM Tris buffer. Note the $\log_{10}$ scale on the vertical axis for panels A through D. (A) Guinier (sphere) plot, graphing scattering intensity (I) as a function of Q^2 (sine of scattering angle). Both monodisperse and polydisperse regions of the curve are evident. (B) Guinier (sphere) plot in the monodisperse region of scattering: $Q^2 = 0.4-0.6$. The fit is characterized by $R = 0.879$. (C) Rod plot, graphing $I*S$ (intensity as a product of scattering angle) as a function of Q^2 (sine of scattering angle). (D) Rod plot for that model in the monodisperse region scattering data ($Q^2 = 0.04-0.06$). The fit is characterized by $R = 0.999$, yielding a transverse radius of gyration of $R_t = \sim 52$ Å for the rod. (E) Histogram of scattering angle ($1/Q$), suggesting that the monodisperse form of CHGA exists in solution.

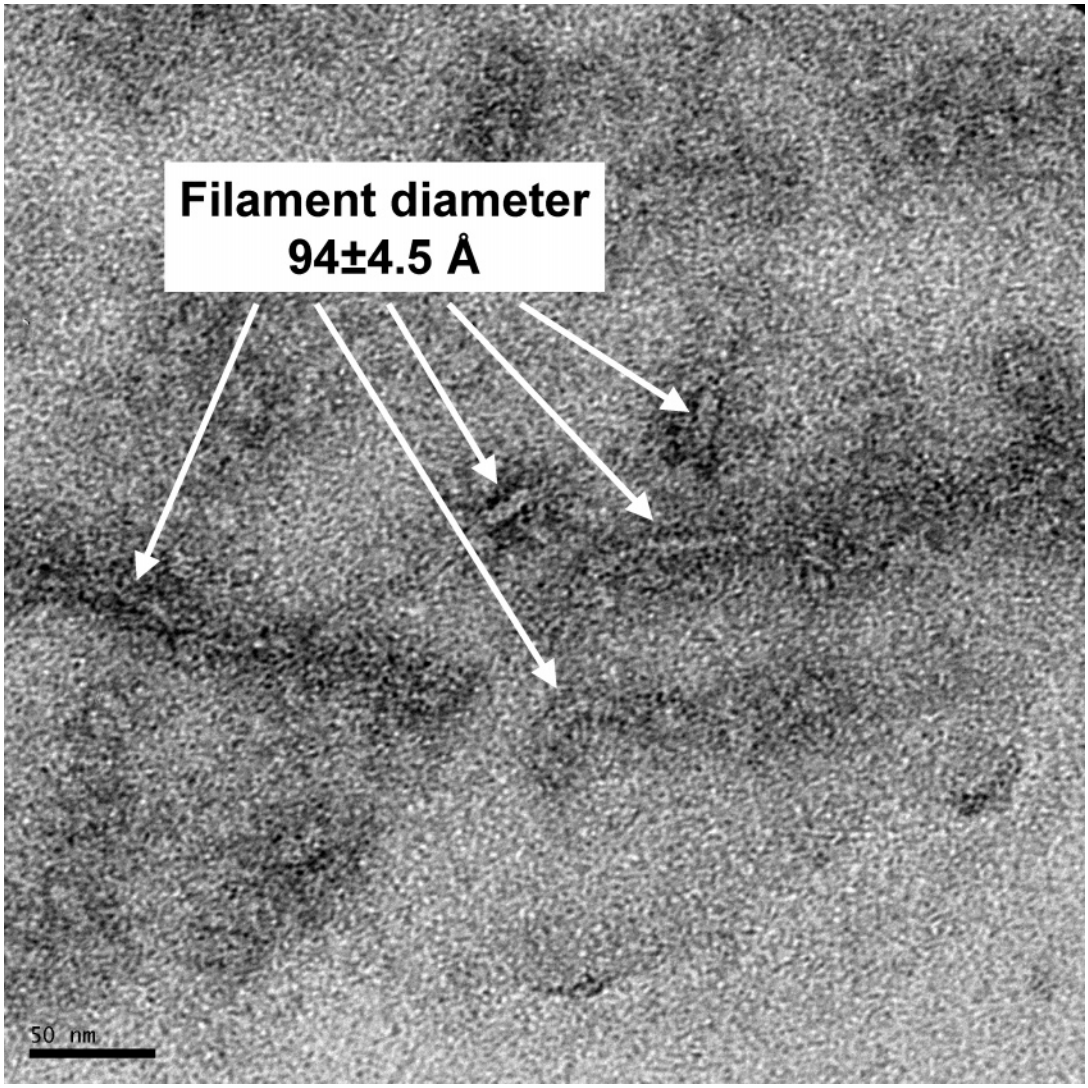

FIGURE 4: Electron microscopy of CHGA. After adsorption of recombinant human CHGA (at 20 mg/mL) to glow-discharged, carbon support films, and negative staining with 1% aqueous uranyl acetate, the grid was examined and images recorded with a FEI Tecnai G2 Sphera electron microscope at 200 kV. The average diameter (14 measurements) of negatively stained protein fibers is shown. The scale bar (lower left-hand corner) indicates 50 nm (500 Å).

proteins. In calibrated images, the width of the filaments was 94 ± 4.5 Å ($n = 14$ cross-sectional measurements on typical filaments). The lengths of the filaments were quite variable, but occasionally >50 nm (>500 Å).

Chromaffin Granule Ultrastructure

Chromaffin granules are intracellular vesicles that are packed with CHGA and catecholamines at high concentrations (*7*−*9*). The electron-dense "packing" of the chromaffin granule core is demonstrated morphologically in Supporting Information Figure VI. This electron micrograph shows both coarsely and finely periodic electron density of the granule cores. The periodicity of the finely granular cores, at 108 ± 6.3 Å, is in the range of the effective Stokes radius (R_S) of ∼84.8 Å for a single CHGA molecule. Since CHGA may bind and thus serve to nucleate a complex including not only cationic catecholamines and calcium (*51*) but also anionic ATP (*52*), one might expect that the diameter of the fundamental repeating unit of organization (108 ± 6.3 Å) within the chromaffin granule core would exceed the effective hydrodynamic dimension of CHGA itself (∼84.8 Å), a prediction compatible with our data. The periodicity of the coarser granular cores is 360 ± 25 Å, which is on the order of ∼4 times the effective CHGA Stokes radius (360 Å/84.8 Å = ∼4.2 times), suggests the possibility of ∼4-fold multimerization of the basic unit of organization of the core. However, these chromaffin granules were prepared after cell disassembly, as is customary, in rather nonphysiological circumstances, including sedimentation through a 1.6 M (hyperosmolar) sucrose gradient (*53*); hence, we cannot exclude a contribution of osmotic artifacts to the pattern of electron density observed in the isolated granules (Supporting Information Figure VI).

Contribution of CHGA to the Formation of the Regulated Exocytotic Secretory Pathway

Chromaffin Cells in Vitro: Exogenous Cotransmitter Exocytosis. Supporting Information Figure VII illustrates the consequences of CHGA ablation for the regulated secretory pathway in chromaffin cells. Introduction of the *CHGA* siRNA reagent dose-dependently decreased expression of CHGA protein in chromaffin cells to ∼5% of control values

(Supporting Information Figure VII-B). By contrast, a negative control siRNA (directed to an irrelevant protein) had no effect (Supporting Information Figure VII-A). We then probed the regulated secretory pathway by triggering exocytosis of transfected/expressed/trafficked growth hormone from chromaffin granules (*1*, *39*). After ablation of CHGA expression, regulated storage and exocytosis of growth hormone was diminished by ~65% (Supporting Information Figure VII-C).

Chromaffin Cells in Vivo: Endogenous Cotransmitter Storage. Targeted ablation of the CHGA gene in mice resulted in substantial (~40−80%) and significant ($p < 0.005$ to $p < 0.0001$) decrements in the concentrations of each endogenous chromaffin granule cotransmitter assayed in the adrenal gland: norepinephrine, epinephrine, neuropeptide Y, and ATP (Supporting Information Figure VII-D).

Other Chromogranin/Secretogranin Protein Family Members Also Bear Homology to Tropomyosin's Coiled-Coil

Application of PSI-BLAST (*54*) also identified homology matches of 3 other human chromogranin/secretogranin family members to tropomyosin (1c1g A-chain): chromogranin B (CHGB), secretogranin II (SCG2), and VGF. Human CHGB matched 1c1g at a likelihood of 1×10^{-7}, over CHGB residues 392−669 (full-length CHGB: 677 residues), corresponding to 1c1g residues 1−280. Human SCG2 matched 1c1g at a likelihood of 8×10^{-5}, over SCG2 residues 1−203 (full-length SCG2: 617 residues), corresponding to 1c1g residues 73−275. Human VGF matched 1c1g at a likelihood of 2×10^{-3}, over VGF residues 1−230 (full-length VGF: 616 residues), corresponding to 1c1g residues 39−277. These homology matches to TPM1 did not achieve the higher level of significance found for human CHGA (at 4×10^{-11}).

Effect of Catestatin Naturally Occurring Genetic Variants on the Coiled-Coil Homology

The entire length of the tropomyosin polypeptide (TPM1 residues 1−284) also displayed homology with CHGA chains bearing naturally occurring non-synonymous cSNP variants within the catecholamine release-inhibitory catestatin region: Gly364Ser, Pro370Leu, and Arg374Gln (4); (*55*). In each case, the match began at CGHA amino acid Ile_{48} and extended into the catestatin domain ($CHGA_{340-372}$; Supporting Information Figure VIII); preservation of the tropomyosin homology across this CHGA region is perhaps not unexpected since the variants are just carboxy-terminal to the matched region. Catestatin itself may have amphiphilic beta-sheet secondary (*43*, *44*) and coiled-loop tertiary (6) structure, and thus be excluded from the coiled-coil motif.

The coiled-coil alignment apparently changed for each catestatin variant, but at some distance from the catestatin domain: the SNP changes at catestatin amino acids Gly364Ser, Pro370Leu, or Arg374Gln each seemed to induce a gap into the tropomyosin/CHGA alignment, wherein the gap excludes a 4 amino acid segment of the pancreastatin ($CHGA_{250-301}$) domain from the coiled-coil homology (Supporting Information Figure II). In the case of CHGA Gly364Ser, an induced homology gap between tropomyosin Glu_{224}↓Ile_{225} (downward arrow indicating the gap) results in coiled-coil exclusion of CHGA $Met_{291}Ala_{292}Val_{293}Val_{294}$; while in the case of either CHGA Pro370Leu or Arg374Gln, an induced homology gap between tropomyosin Ile_{225}↓Lys_{226} results in coiled-coil exclusion of CHGA $Ala_{292}Val_{293}Val_{294}Pro_{295}$.

Similar analyses of 8 additional, naturally occurring non-synonymous SNPs spanning CHGA (Glu71Gly, Glu158Lys, Glu246Asp, Arg253Trp, Ala256Gly, Leu314Pro, Gly297Ser, and Arg381Trp) (*4*) were undertaken. Glu71Gly did not affect the wild-type homology model. However, each of the other SNPs resulted in exclusion of 4 amino acids from the coiled-coil in the pancreastatin domain, either $Met_{291}-Val_{294}$ (by Glu158Lys, Gly297Ser, or Leu314Pro), or $Ala_{292}-Pro_{295}$ (by Arg253Trp, Ala256Gly, or Arg381Trp). Of note, three polymorphisms (Arg253Trp, Ala256Gly, Gly297Ser) within the pancreastatin domain ($CHGA_{250-301}$) seemed to affect the coiled-coil structure in that same region ($Met_{291}-Pro_{295}$).

DISCUSSION

Overview. The rapid proliferation of genome sequencing far outpaces the ability to establish 3-dimensional structures via crystallography or NMR; indeed, the entire $\sim 3.3 \times 10^9$ bp human genome has been almost completely sequenced, yielding up to ~35,000 protein-encoding genes (*56*). Nonetheless, 3-D structures have profound implications for elucidating functional models of proteins. Proteome-wide approaches (*12*) now allow species-specific assignment of putative structural homologues within over 100 proteomes from publicly available data (see <eol.sdsc.edu>). Here we characterize a homology structure for the secretory granule core protein CHGA, in which the predicted coiled-coil structure successfully accounts for several unusual physical properties of the protein.

CHGA as a Coiled-Coil Structure: Evidence and Implications. Tropomyosin and other coiled-coils have a characteristic repeating pattern of seven amino acid residues residues (a → g heptad), wherein residues a and d are hydrophobic (*24*, *42*). The nonintegral (every ~3.5 residue) nature of the pitch of the helix results in a hydrophobic residue side-chain "stripe" winding along the length of the helix, prompting the two interacting helices to wind around one another, forming a left-handed supercoil, or coiled-coil (*24*).

The *e* (expectation)- and *z*-values chosen to establish the reliability of homology matches were confirmed separately for the proteome of each species (*12*). To understand whether the CHGA/TPM1 homology was general (across species), we first submitted a BLAST search for the wild-type mature human CHGA against all proteins in the EOL database (*12*). There are CHGA proteins from 6 mammalian species (including human) whose known proteomes have been processed via the EOL PSI-BLAST and/or 123D routines (*12*) (Table 1). Using the mature human CHGA protein of 439 amino acids as the baseline, the other species CHGA-to-CHGA alignments ranged from 421 (rat) to 445 (mouse) amino acids in length. Table 1 lists CHGA for several species (column 1) in decreasing sequence homology compared to human, with the number of identical amino acids listed in column 3. Equine CHGA is the closest and rat the most distant of these species. The amino acid homology/fold match occurred between human $CHGA_{48-349}$ and the entire tropomyosin chain of 284 amino acids. There was a similar amino acid span for the human, equine, bovine, porcine, and rat CHGA homologies to tropomyosin, as listed in column

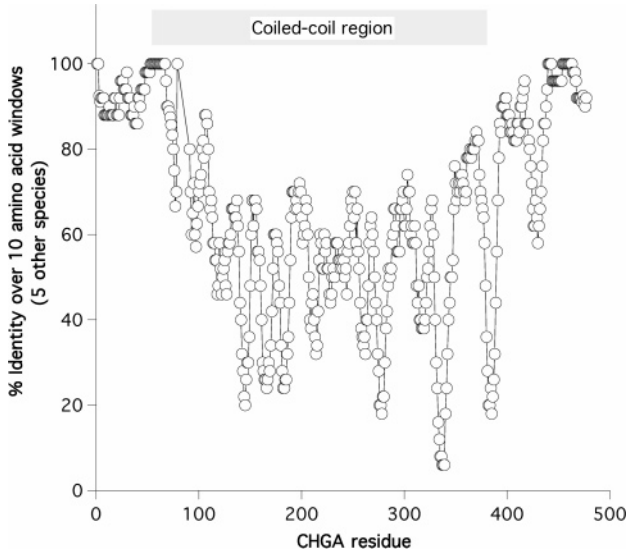

FIGURE 5: Chromogranin A interspecies sequence homology and coiled-coil domain. CHGA primary structure across 6 mammalian species was evaluated by noting the % sequence identity (0−100%) with human CHGA. After alignment of 6 species' (human, bovine, equine, porcine, rat, mouse) CHGAs by Clustal-W (version 1.83) <http://www.ebi.ac.uk/clustalw/>, the results of average identity over sliding windows of 10 amino acids are plotted. The region of coiled-coil homology is shown at the top. Although the mature human CHGA is $CHGA_{1-439}$, because of interspecies alignment "gaps" the number of amino acids on the horizontal axis is 477.

6 of Table 1. These five species' CHGAs matched tropomyosin via 123D, despite the decreasing sequence CHGA-to-CHGA homology on BLAST scores. The level of 123D reliability was "A" or "B" across human/pig/horse/bovine/rat CHGAs, consistent with the "benchmarking" process in the EOL wherein "accuracy" values are separately established for the proteome of each species (*20*) (see Experimental Procedures).

Murine CHGA did not match tropomyosin at reliability of "C" or above, but matched the family member meromyosin over a similar span of amino acids (murine $CHGA_{57-346}$). This match was via PSI-BLAST with a reliability of "C". The portion of chicken meromyosin (PDB ID 1i84) molecule that murine CHGA matched is the extended alpha-helical domain of meromyosin (*57*).

Thus each of the various species' CHGA proteins is predicted to match an extended alpha-helical coiled-coil, via the EOL (PSI-BLAST and/or 123D) algorithms. The retention of the 123D alignment from different species' CHGA to tropomyosin (Table 1), even as the sequence alignment between that species' CHGA and human CHGA diminished, demonstrates the preservation of secondary and tertiary structural homology across species. The 123D homology matches of greatest reliability ("A" score, ≥99.9% fold assignment accuracy) were for pig and horse CHGAs. Even though the X-ray crystal structure for full-length tropomyosin at highest resolution (~7 Å) is solved for the porcine molecule (PDB 1c1g) (*42*), multiple mammalian species CHGAs (Table 1) displayed homology matches to 1c1g at high reliability. Figure 5 illustrates interspecies sequence identity among six mammalian CHGAs, across the entire protein. Of note, the coiled-coil domain of CHGA is found in the mid-molecule (human $CHGA_{48-349}$), a region of only modest interspecies sequence conservation (Figure 5) as compared to the better-conserved amino- and carboxyl-termini. Thus, the secondary and tertiary structural motif of the coiled-coil (Figure 1; Supporting Information Figure I) seems to be conserved even in a region of diminishing primary structural identity; since a coiled-coil requires only the repetition of a heptad (a → g) with hydrophobic residues at heptad positions a and d (*24*), rather than specific amino acids at particular heptad positions, the coil's retention even in areas of declining interspecies sequence conservation does not violate expectations.

Like tropomyosin, CHGA can homodimerize, and even form homotetramers (*14*, *15*); of note, a tetramer is the characteristic coiled-coil form of tropomyosin (*42*). Tropomyosin coils in a parallel manner within each of the coiled-coil homodimers, while two such homodimers align in antiparallel fashion to form the homotetramer; thus, we would model a CHGA coiled-coil in a similar "stacking" fashion, with particular implications for its very dense "packing" within the core of chromaffin granules (*7*−*9*).

Although the previously characterized homodimerization of CHGA may involve its intramolecular disulfide bridge, spanning residues Cys_{17}−Cys_{38} (*39*, *58*), intriguingly this hydrophobic loop motif is not included within the predicted extended coiled-coil domain ($CHGA_{48-349}$; i.e., Ile_{48} through Asn_{349}). Thus, the coiled-coil model provides an alternate mechanism for homomultimerization of CHGA.

The hydrophobic residue side-chain "stripe" of a coiled-coil might also provide a surface for interaction of CHGA with membrane components of the regulated secretory pathway; indeed, the His_{79}−Leu_{90} region of human CHGA (H_{79}SG**F**EDE**L**SEV**L**$_{90}$) conforms exactly (12/12 match) to three turns of a putative amphipathic alpha-helical motif, wherein hydrophobic residues (in bold type) occur every at fourth residue in the primary structure, and lies within a domain necessary for trafficking of CHGA into the regulated secretory pathway (*24*). Perhaps such a discrete segment of CHGA could be recognized as a sorting determinant to the regulated pathway, by virtue of its putative membrane interaction.

Implications of CHGA Polymorphism for Coiled-Coil Homology. We noted that the region of predicted CHGA coiled-coil seemed to vary as a function of naturally occurring (4) functional (*55*) polymorphism in the catestatin region (Supporting Information Figure VIII). In particular, each catestatin variant seemed to induce a 4 amino acid exclusion from coiled-coil homology (at CHGA resides $Met_{291}Ala_{292}Val_{293}Val_{294}Pro_{295}$), within the carboxy-terminal active region of the pancreastatin domain ($CHGA_{250-301}$) in human CHGA (*59*). Of note, because of its cyclic imino acid ring in the peptide backbone, Pro_{295} would already be predicted to destabilize any alpha-helical region (*60*). What might be the implications of this polymorphism-induced change in secondary structure at the pancreastatin region? First of all, the overall conformation of CHGA might become less compact, leading to decrements of chromaffin granule transmitter storage density and exocytotic release in subjects with catestatin variants. Second, the carboxy-terminal recognition site for pancreastatin processing (cleavage and amidation signals at $Gly_{301}Gly_{302}Lys_{303}$) might become more surface-accessible to the processing enzymes in the chromaffin granule core. These possible structural implications might be tested in recombinant CHGA, or in humans

stratified by catestatin variant genotypes (Gly364Ser, Pro370Leu, or Arg374Gln).

Physical Properties of CHGA Compatible with Coiled-Coil Structure. Using a proteome-wide approach to protein folding (*12*), we discovered a structural homologue (tropomyosin) for a molecule (CHGA) that has not been crystallized, and then provided substantial new experimental evidence in support of this prediction (Figures 2, 3, 4; Supporting Information Figure IV).

The results of native gel filtration studies show an unexpectedly high apparent molecular weight of M_{app} ~578 kDa (Supporting Information Figure IVB) and a Stokes radius of ~84.8 Å, despite a predicted R_S ~30 Å based on an actual molecular mass of ~49 kDa. Even though CHGA may homodimerize or even homotetramerize (*12*, *14*, *15*, *58*), the M_{app} of ~578 kDa would then suggest >10-fold multimerization; alternatively, a rather unusual, extended conformation is entirely compatible with our homology model (Supporting Information Figure II).

The coiled-coil domain predictions (Figure 1; Supporting Information Figure II) and CD spectra (Figure 2) indicate that CHGA does assume such an alpha-helical and then coiled-coil conformation. Historically, the extended structure predicted by homology modeling is also consistent with the unusual (early) gel filtration elution and optical rotatory dispersion properties noted for bovine CHGA (*13*, *61*), as well as similarly high ratios of polar to nonpolar amino acids for CHGA and tropomyosin (*13*). An early NMR structure also suggested an extended conformation for bovine CHGA (*62*). The presence of alpha-helix within CHGA has also been documented previously for bovine CHGA (*61*).

During SAXS (Figure 3), CHGA displayed a range of self-association (Figure 6A and 6C), though the monomeric form was the quantitatively most prominent (Figure 3E). When X-ray scattering behavior in the monodisperse range was evaluated, the data best fit the model for a rod-like structure (Figure 3D, $R = 0.999$), with the transverse radius of gyration of the cylinder estimated at R_t = ~52 Å. This value is somewhat greater than the observed stacking periodicity of coiled-coils within tropomyosin 1c1g crystals at ~20−22 Å (*62*), perhaps consistent with the notion that SAXS observes hydrated molecules freely moving in aqueous solution; by contrast, a crystal is likely to have a far more rigid/fixed packing architecture of defined periodicity. Alternatively, since coiled-coils can exist with up to 7 alpha-helices supercoiled about one another (*63*), the increase in radius from multiple intertwined coils might in part account for the R_t = ~52 Å that we found (Figure 6D). In any case, the ~52 Å transverse radius of CHGA (Figure 3D) is substantially greater than the radius predicted for a simple alpha-helix at ~5−10 Å (depending upon the nature of the side chains).

Many of our SAXS experiments on CHGA (Figure 3) were performed at relatively high protein concentration (20 mg/mL, or ~400 μM), while the CD experiments (Figure 2) were performed at lower protein concentration (300 mg/L, or ~5 μM). The protein concentrations were chosen based on optimal spectral performance of the two different techniques. During SAXS, we did study CHGA at concentrations down to ~100 μM, and noted a qualitatively similar scattering profile suggesting a continuum of monodisperse to polydisperse forms. Nonetheless, we did not study identical concentrations with the two techniques (CD and SAXS); since the concentration of chromogranins within the chromaffin granule core *in situ* may be as high as ~200 mg/mL (*7*−*9*), higher protein concentrations may better approximate conformations and events *in vivo*.

Electron microscopy of CHGA (Figure 4) revealed elongated filamentous structures with an average diameter of ~94 ± 4.5 Å, which is in the range of the diameter value expected for a cylinder with a radius of ~52 Å (Figure 3D). During transmission EM, 3-dimensional structures may "flatten" as a result of vacuum drying and electron bombardment (*64*, *65*); the degree of increase in particle width from flattening has been reported at ~19−34%, when compared to native 3-dimensional width (*65*, *66*). If so, the native width of the CHGA filaments may actually be in the range of ~70−79 Å. Of note is a previous report that the filament width of fibrinogen, another markedly asymmetric protein, has been reported at ~90 Å during cryo-EM, which avoids artifactual flattening (*67*, *68*).

Chromaffin Granule Ultrastructure. Transmission electron microscopy of freshly isolated human chromaffin granules (Supporting Information Figure VI) revealed periodic patterns of electron density in the soluble cores: a finer periodicity of 108 ± 6.3 Å, and a coarser periodicity of 360 ± 25 Å. This periodic electron density suggests that the granule core may be at least loosely structured rather than a simple solution. Indeed, the very high *in situ* concentrations of granule core solutes (chromogranins at ~200 mg/mL, catecholamines at ~600 mM, ATP at ~150 mM) (*7*−*9*) represent severe departures from physical ideality (*69*), and the effective ionic concentrations (activities) are likely to be far lower than the actual concentrations. Might these concentrations exceed solubility, especially in the progressively low pH/high Ca^{2+} milieu of the mature granule (*1*, *51*)? If so, the unit of nucleation of the granule core complex might be expected to yield a periodic structure to the core. Indeed, we noted a finely granular 108 ± 6.3 Å periodicity, perhaps consistent with the nucleation of a core complex by the ~84.8 Å radius CHGA, with subsequent higher order nucleation to a 360 ± 25 Å complex, suggesting ~4-fold multimerization. Indeed, noncovalent tetramerization of CHGA has been observed *in vitro* (*14*, *58*). While the presence of CHGA as the nucleating factor in such complexes is not established, the binding of multiple granule soluble components by CHGA has been demonstrated (*51*, *52*), and genetic ablation of CHGA *in vivo* clearly diminishes the size, number, and electron density of adrenal chromaffin granules (*40*).

Implications for Chromaffin Granule Biogenesis and Regulated Secretory Protein Trafficking. The transmission electron micrograph (Supporting Information Figure VI) demonstrates the electron-dense core packing of granule contents, including CHGA. Indeed, the chromaffin granule core is known to contain its soluble cargo at very high concentrations, in a physical matrix whose activities deviate substantially from physical ideality: chromogranins (the major one being CHGA) at ~200 mg/mL, catecholamines at ~600 mM, and ATP at ~150 mM (*7*−*9*).

What are the implications of a coiled-coil, versus a globular/spherical structure, for the density of the chromaffin granule core? The solid geometry of such structures is potentially quite different. If a rod or cylinder (rod volume

$= \pi r^2 h$) approximates the potential "packing" density of a linear alpha-helix (or coiled-coil), versus a sphere (sphere volume $= (4/3)\pi r^3$) for a globular protein, then a coiled-coil would allow the protein to occupy up to ~78.5% of the available 3-dimensional space, versus only ~52.4% for a globular/spherical protein. In principle, then, a coiled-coil structure could allow the accumulation of the secretory granule core proteins (chromogranins/secretogranins) to ~1.5-fold (= 78.5/52.4) higher concentrations than might otherwise occur. Thus, the coiled-coil structure of the major granule core protein (CHGA) might contribute to its extraordinary condensation (to ~200 mg/mL) within the soluble core, an event that may nucleate the condensation of cotransmitters such as other peptide hormones, catecholamines, and ATP. Consistent with this viewpoint, depletion of endogenous CHGA, either in cultured chromaffin cells (*70*, *71*) or in the adrenal medulla of mice with targeted ablation of the *CHGA* gene (*40*), results in a systematic decline in chromaffin granule number, size, and electron density (*40*).

Indeed, inhibition of CHGA expression in chromaffin cells by siRNA (Supporting Information Figure VII-A/B/C) disrupted chromaffin granule regulated secretory protein trafficking and exocytosis by ~65%, while chromaffin granule cotransmitter concentrations were depleted by ~40−80% after targeted ablation of the CHGA gene in the mouse (Supporting Information Figure VII-D).

What is the significance of the CHGA regions at its amino- and carboxy-termini, that are not likely to form coiled-coils (Figure 5)? The CHGA region homologous to tropomyosin starts at residue Ile_{48}, past the disulfide loop (Cys_{17}−Cys_{39}) that may be critical for vesicular trafficking (*39*, *58*), and ends at residue Asn_{349}, within the catestatin moiety ($CHGA_{340-372}$) and its amino-terminal dibasic cleavage residues $Lys_{338}Arg_{339}$ (*31*, *72*). The CHGA fragment vasostatin spans amino acids 1−76 of the mature CHGA protein (*45*). Thus the extended alpha-helical/coiled-coil model of CHGA (Figure 2) allows the central polypeptide chain (Ile_{48} through Asn_{349}) to be closely packed, but leaves the biologically active peptide-encoding termini accessible to proteolytic cleavage. In analogous fashion, tropomyosin is most densely packed in its central coiled-coil configuration, with the end structures modulating the coil's stability (*73*).

Finally, significant homology matches to tropomyosin (1c1g) for 3 other members of the chromogranin/secretogranin protein family (CHGB, SCG2, and VGF) raise the possibility of coiled-coil heterodimerization among the chromogranins within the secretory granule core, extending the likelihood of very dense packing to other members of the granin family, and accommodating the diversity in granin composition across different secretory granule anatomic sites within the neuroendocrine system (*45*).

CONCLUSIONS AND PERSPECTIVES

A novel prediction of significant structural homology, with extended coiled-coil features, between CHGA and tropomyosin is supported by the new physicochemical evidence presented on the unusual conformation of CHGA in solution. The novel CHGA homology model predicts several otherwise difficult-to-explain physical features of the CHGA molecule, and suggests a mechanism for dense secretory protein packing during the biogenesis of the chromaffin granule core. Future studies will probe the functional significance of this unexpected structural feature of CHGA, including its dependence upon the particular ionic conditions (i.e., the granule interior milieu of low pH and high Ca^{2+}) (*1*, *51*) that occur during secretory granule nucleation and maturation.

ACKNOWLEDGMENT

We thank our colleagues at the EOL (Encyclopedia Of Life) Project—Philip Bourne, Ilya Shindyalov, Wilfred Li, Vicente Reyes, Robert Byrnes and Greg Quinn—for developing the annotation pipeline, making their data available, and providing training in its use. Portions of this research were carried out at the Stanford Synchrotron Radiation Laboratory (SSRL). At SSRL, Thomas Weiss and Hiro Tsuruta assisted us in the experiments. We acknowledge the assistance of the UCSD Cryo-Electron Microscopy Facility <http://cryoem.ucsd.edu/>. We appreciate helpful discussions with Dr. Gerald Stubbs at Vanderbilt University on approaches to coiled-coil structure determination.

SUPPORTING INFORMATION AVAILABLE

Figures I through VIII as described in the text. This material is available free of charge via the Internet at http://pubs.acs.org.

REFERENCES

1. Taupenot, L., Harper, K. L., and O'Connor, D. T. (2005) Role of H^+-ATPase-mediated acidification in sorting and release of the regulated secretory protein chromogranin A: evidence for a vesiculogenic function, *J. Biol. Chem. 280*, 3885−3897.
2. Parmer, R. J., Koop, A. H., Handa, M. T., and O'Connor, D. T. (1989) Molecular cloning of chromogranin A from rat pheochromocytoma cells, *Hypertension 14*, 435−444.
3. Wu, H. J., Rozansky, D. J., Parmer, R. J., Gill, B. M., and O'Connor, D. T. (1991) Structure and function of the chromogranin A gene. Clues to evolution and tissue-specific expression, *J. Biol. Chem. 266*, 13130−13134.
4. Wen, G., Mahata, S. K., Cadman, P., Mahata, M., Ghosh, S., Mahapatra, N. R., Rao, F., Stridsberg, M., Smith, D. W., Mahboubi, P., et al. (2004) Both rare and common polymorphisms contribute functional variation at CHGA, a regulator of catecholamine physiology, *Am. J. Hum. Genet. 74*, 197−207.
5. O'Connor, D. T., Kailasam, M. T., Kennedy, B. P., Ziegler, M. G., Yanaihara, N., and Parmer, R. J. (2002) Early decline in the catecholamine release-inhibitory peptide catestatin in humans at genetic risk of hypertension, *J. Hypertens. 20*, 1335−1345.
6. Preece, N. E., Nguyen, M., Mahata, M., Mahata, S. K., Mahapatra, N. R., Tsigelny, I., and O'Connor, D. T. (2004) Conformational preferences and activities of peptides from the catecholamine release-inhibitory (catestatin) region of chromogranin A, *Regul. Pept. 118*, 75−87.
7. Winkler, H., and Fischer-Colbrie, R. (1998) Regulation of the biosynthesis of large dense-core vesicles in chromaffin cells and neurons, *Cell. Mol. Neurobiol. 18*, 193−209.
8. Winkler, H., and Fischer-Colbrie, R. (1992) The chromogranins A and B: the first 25 years and future perspectives, *Neuroscience 49*, 497−528.
9. Phillips, J. H. (1982) Dynamic aspects of chromaffin granule structure, *Neuroscience 7*, 1595−1609.
10. Moult, J., Fidelis, K., Zemla, A., and Hubbard, T. (2001) Critical assessment of methods of protein structure prediction (CASP): round IV, *Proteins Suppl. 5*, 2−7.
11. Li, W. W., Quinn, G. B., Alexandrov, N. N., Bourne, P. E., and Shindyalov, I. N. (2003) A comparative proteomics resource: proteins of Arabidopsis thaliana, *Genome Biol. 4*, R51.
12. Li, W. W., Byrnes, R., Hayes, J., Reyes, V., Birnbaum, A., Shahab, A., Mosley, C., Pekurovsky, D., Quinn, G. B., Shindyalov, I., et al. (2004) The Encyclopedia of Life Project: Grid Software and Deployment, *Grid Syst. Life Sci. 22*, 127−136.

13. Smith, A. D., and Winkler, H. (1967) Purification and properties of an acidic protein from chromaffin granules of bovine adrenal medulla, *Biochem. J. 103*, 483−492.
14. Yoo, S. H., and Lewis, M. S. (1992) Effects of pH and Ca^{2+} on monomer-dimer and monomer-tetramer equilibria of chromogranin A, *J. Biol. Chem. 267*, 11236−11241.
15. Yoo, S. H., and Lewis, M. S. (1996) Effects of pH and Ca^{2+} on heterodimer and heterotetramer formation by chromogranin A and chromogranin B, *J. Biol. Chem. 271*, 17041−17046.
16. Veretnik, S., Bourne, P. E., Alexandrov, N. N., and Shindyalov, I. N. (2004) Toward consistent assignment of structural domains in proteins, *J. Mol. Biol. 339*, 647−678.
17. Altschul, S. F., Madden, T. L., Schaffer, A. A., Zhang, J., Zhang, Z., Miller, W., and Lipman, D. J. (1997) Gapped BLAST and PSI-BLAST: a new generation of protein database search programs, *Nucleic Acids Res. 25*, 3389−3402.
18. Alexandrov, N. N., Nussinov, R., and Zimmer, R. M. (1996) Fast protein fold recognition via sequence to structure alignment and contact capacity potentials, *Pac. Symp. Biocomput*. 53−72.
19. Alexandrov, N., and Shindyalov, I. (2003) PDP: protein domain parser, *Bioinformatics 19*, 429−430.
20. Shindyalov, I. N., Alexandrov, N. N., and Bourne, P. E. (2006) What to expect from an expectation value, *Bioinformatics*, submitted.
21. Sali, A., and Blundell, T. L. (1993) Comparative protein modelling by satisfaction of spatial restraints, *J. Mol. Biol. 234*, 779−815.
22. Rost, B., and Sander, C. (1993) Prediction of protein secondary structure at better than 70% accuracy, *J. Mol. Biol. 232*, 584−599.
23. Rost, B., Yachdav, G., and Liu, J. (2004) The PredictProtein server, *Nucleic Acids Res. 32*, W321−326.
24. Lupas, A., Van Dyke, M., and Stock, J. (1991) Predicting coiled coils from protein sequences, *Science 252*, 1162−1164.
25. O'Connor, D. T., Frigon, R. P., and Sokoloff, R. L. (1984) Human chromogranin A. Purification and characterization from catecholamine storage vesicles of human pheochromocytoma, *Hypertension 6*, 2−12.
26. O'Connor, D. T., and Frigon, R. P. (1984) Chromogranin A, the major catecholamine storage vesicle soluble protein. Multiple size forms, subcellular storage, and regional distribution in chromaffin and nervous tissue elucidated by radioimmunoassay, *J. Biol. Chem. 259*, 3237−3247.
27. Syversen, U., Waldum, H. L., and O'Connor, D. T. (1992) Rapid, high-yield isolation of human chromogranin A from chromaffin granules of pheochromocytomas, *Neuropeptides 22*, 235−240.
28. Kruggel, W., O'Connor, D. T., and Lewis, R. V. (1985) The amino terminal sequences of bovine and human chromogranin A and secretory protein I are identical, *Biochem. Biophys. Res. Commun. 127*, 380−383.
29. Fish, W. W., Mann, K. G., and Tanford, C. (1969) The estimation of polypeptide chain molecular weights by gel filtration in 6 M guanidine hydrochloride, *J. Biol. Chem. 244*, 4989−4994.
30. Fish, W. W., Reynolds, J. A., and Tanford, C. (1970) Gel chromatography of proteins in denaturing solvents. Comparison between sodium dodecyl sulfate and guanidine hydrochloride as denaturants, *J. Biol. Chem. 245*, 5166−5168.
31. Taylor, C. V., Taupenot, L., Mahata, S. K., Mahata, M., Wu, H., Yasothornsrikul, S., Toneff, T., Caporale, C., Jiang, Q., Parmer, R. J., et al. (2000) Formation of the catecholamine release-inhibitory peptide catestatin from chromogranin A. Determination of proteolytic cleavage sites in hormone storage granules, *J. Biol. Chem. 275*, 22905−22915.
32. Kelly, S. M., and Price, N. C. (1997) The application of circular dichroism to studies of protein folding and unfolding, *Biochim. Biophys. Acta 1338*, 161−185.
33. Andrade, M. A., Chacon, P., Merelo, J. J., and Moran, F. (1993) Evaluation of secondary structure of proteins from UV circular dichroism spectra using an unsupervised learning neural network, *Protein Eng. 6*, 383−390.
34. Merelo, J. J., Andrade, M. A., Prieto, A., and Moran, F. (1994) Proteinotopic Feature Maps, *Neurocomputing 6*, 443−454.
35. Tsuruta, H., Brennan, S., Rek, Z. U., Irving, T. C., Tompkins, W. H., and Hodgson, K. O. (1998) A Wide Bandpass Multilayer Monochromator for Biological Small Angle Scattering and Fiber Diffraction Studies, *J. Appl. Crystallogr. 31*, 672−682.
36. Tsuruta, H., Vachette, P., and Kantrowitz, E. R. (1998) Direct observation of an altered quaternary-structure transition in a mutant aspartate transcarbamoylase, *Proteins 31*, 383−390.
37. Vachette, P., and Svergun, D. Small-Angle X-Ray Scattering By Solutions of Biological Macromoledules, in *Structure and Dynamics of Biomolecules* (Fanchon, E., Geissler, G., Hodeau, J.-L., Regnard, R., and Timmins, P. A., Eds.) pp 199−237, Oxford University Press, New York.
38. Koch, M. H., Vachette, P., and Svergun, D. I. (2003) Small-angle scattering: a view on the properties, structures and structural changes of biological macromolecules in solution, *Q. Rev. Biophys. 36*, 147−227.
39. Taupenot, L., Harper, K. L., Mahapatra, N. R., Parmer, R. J., Mahata, S. K., and O'Connor, D. T. (2002) Identification of a novel sorting determinant for the regulated pathway in the secretory protein chromogranin A, *J. Cell Sci. 115*, 4827−4841.
40. Mahapatra, N. R., O'Connor, D. T., Vaingankar, S. M., Hikim, A. P., Mahata, M., Ray, S., Staite, E., Wu, H., Gu, Y., Dalton, N., et al. (2005) Hypertension from targeted ablation of chromogranin A can be rescued by the human ortholog, *J. Clin. Invest. 115*, 1942−1952.
41. Kennedy, B., and Ziegler, M. G. (1990) A more sensitive and specific radioenzymatic assay for catecholamines, *Life Sci. 47*, 2143−2153.
42. Whitby, F. G., and Phillips, G. N., Jr. (2000) Crystal structure of tropomyosin at 7 Angstroms resolution, *Proteins 38*, 49−59.
43. Kennedy, B. P., Mahata, S. K., O'Connor, D. T., and Ziegler, M. G. (1998) Mechanism of cardiovascular actions of the chromogranin A fragment catestatin in vivo, *Peptides 19*, 1241−1248.
44. Tsigelny, I., Mahata, S. K., Taupenot, L., Preece, N. E., Mahata, M., Khan, I., Parmer, R. J., and O'Connor, D. T. (1998) Mechanism of action of chromogranin A on catecholamine release: molecular modeling of the catestatin region reveals a beta-strand/loop/beta-strand structure secured by hydrophobic interactions and predictive of activity, *Regul. Pept. 77*, 43−53.
45. Taupenot, L., Harper, K. L., and O'Connor, D. T. (2003) The chromogranin-secretogranin family, *N. Engl. J. Med. 348*, 1134−1149.
46. Gadroy, P., Stridsberg, M., Capon, C., Michalski, J. C., Strub, J. M., Van Dorsselaer, A., Aunis, D., and Metz-Boutigue, M. H. (1998) Phosphorylation and O-glycosylation sites of human chromogranin A (CGA79−439) from urine of patients with carcinoid tumors, *J. Biol. Chem. 273*, 34087−34097.
47. Barbosa, J. A., Gill, B. M., Takiyyuddin, M. A., and O'Connor, D. T. (1991) Chromogranin A: posttranslational modifications in secretory granules, *Endocrinology 128*, 174−190.
48. Konecki, D. S., Benedum, U. M., Gerdes, H. H., and Huttner, W. B. (1987) The primary structure of human chromogranin A and pancreastatin, *J. Biol. Chem. 262*, 17026−17030.
49. Greenfield, N. J., Stafford, W. F., and Hitchcock-DeGregori, S. E. (1994) The effect of N-terminal acetylation on the structure of an N-terminal tropomyosin peptide and alpha alpha-tropomyosin, *Protein Sci. 3*, 402−410.
50. Perry, S. V. (2001) Vertebrate tropomyosin: distribution, properties and function, *J. Muscle Res. Cell Motil. 22*, 5−49.
51. Videen, J. S., Mezger, M. S., Chang, Y. M., and O'Connor, D. T. (1992) Calcium and catecholamine interactions with adrenal chromogranins. Comparison of driving forces in binding and aggregation, *J. Biol. Chem. 267*, 3066−3073.
52. Berneis, K. H., Goetz, U., Da Prada, M., and Pletscher, A. (1973) Interaction of aggregated catecholamines and nucleotides with intragranular proteins, *Naunyn-Schmiedeberg's Arch. Pharmacol. 277*, 291−296.
53. Smith, A. D., and Winkler, H. (1967) A simple method for the isolation of adrenal chromaffin granules on a large scale, *Biochem. J. 103*, 480−482.
54. Pieper, U., Eswar, N., Braberg, H., Madhusudhan, M. S., Davis, F. P., Stuart, A. C., Mirkovic, N., Rossi, A., Marti-Renom, M. A., Fiser, A., et al. (2004) MODBASE, a database of annotated comparative protein structure models, and associated resources, *Nucleic Acids Res. 32*, D217−222.
55. Mahata, S. K., Mahata, M., Wen, G., Wong, W. B., Mahapatra, N. R., Hamilton, B. A., and O'Connor, D. T. (2004) The catecholamine release-inhibitory "catestatin" fragment of chromogranin A: naturally occurring human variants with different potencies for multiple chromaffin cell nicotinic cholinergic responses, *Mol. Pharmacol. 66*, 1180−1191.
56. Lander, E. S., Linton, L. M., Birren, B., Nusbaum, C., Zody, M. C., Baldwin, J., Devon, K., Dewar, K., Doyle, M., FitzHugh, W., et al. (2001) Initial sequencing and analysis of the human genome, *Nature 409*, 860−921.

57. Wendt, T., Taylor, D., Trybus, K. M., and Taylor, K. (2001) Three-dimensional image reconstruction of dephosphorylated smooth muscle heavy meromyosin reveals asymmetry in the interaction between myosin heads and placement of subfragment 2, *Proc. Natl. Acad. Sci. U.S.A. 98*, 4361−4366.
58. Thiele, C., and Huttner, W. B. (1998) The disulfide-bonded loop of chromogranins, which is essential for sorting to secretory granules, mediates homodimerization, *J. Biol. Chem. 273*, 1223−1231.
59. O'Connor, D. T., Cadman, P. E., Smiley, C., Salem, R. M., Rao, F., Smith, J., Funk, S. D., Mahata, S. K., Mahata, M., Wen, G., et al. (2005) Pancreastatin: multiple actions on human intermediary metabolism in vivo, variation in disease, and naturally occurring functional genetic polymorphism, *J. Clin. Endocrinol. Metab. 90*, 5414−5425.
60. Kim, M. K., and Kang, Y. K. (1999) Positional preference of proline in alpha-helices, *Protein Sci. 8*, 1492−1499.
61. Yoo, S. H., and Albanesi, J. P. (1990) $Ca^{2(+)}$-induced conformational change and aggregation of chromogranin A, *J. Biol. Chem. 265*, 14414−14421.
62. Daniels, A. J., Williams, R. J., and Wright, P. E. (1978) The character of the stored molecules in chromaffin granules of the adrenal medulla: a nuclear magnetic resonance study, *Neuroscience 3*, 573−585.
63. Liu, J., Zheng, Q., Deng, Y., Cheng, C. S., Kallenbach, N. R., and Lu, M. (2006) A seven-helix coiled coil, *Proc. Natl. Acad. Sci. U.S.A. 103*, 15457−15462.
64. Jesior, J. C., and Wade, R. H. (1987) Electron-irradiation-induced flattening of negatively stained 2D protein crystals, *Ultramicroscopy 21*, 313−319.
65. Serwer, P. (1977) Flattening and shrinkage of bacteriophage T7 after preparation for electron microscopy by negative staining, *J. Ultrastruct. Res. 58*, 235−243.
66. van Antwerpen, R., Chen, G. C., Pullinger, C. R., Kane, J. P., LaBelle, M., Krauss, R. M., Luna-Chavez, C., Forte, T. M., and Gilkey, J. C. (1997) Cryo-electron microscopy of low density lipoprotein and reconstituted discoidal high density lipoprotein: imaging of the apolipoprotein moiety, *J. Lipid Res. 38*, 659−669.
67. Estis, L. F., and Haschemeyer, R. H. (1980) Electron microscopy of negatively stained and unstained fibrinogen, *Proc. Natl. Acad. Sci. U.S.A. 77*, 3139−3143.
68. Bachmann, L., Schmitt-Furnian, W. W., Hammel, R., and Lederer. (1975) Grosse und Gestalt von Fibrinogen. 1. Mitt. Elektronenmikroskopie des hydratisierten Molekuls, *Makromol. Chem.* 2603−2618.
69. Tinoco, I., Sauer, K., Wang, J. C., and Puglisi, J. D. (2001) *Physical Chemistry: Principles and Applications in Biological Sciences*, 740 pp, Prentice Hall, Upper Saddle River, NJ.
70. Kim, T., Tao-Cheng, J. H., Eiden, L. E., and Loh, Y. P. (2001) Chromogranin A, an "on/off" switch controlling dense-core secretory granule biogenesis, *Cell 106*, 499−509.
71. Huh, Y. H., Jeon, S. H., and Yoo, S. H. (2003) Chromogranin B-induced secretory granule biogenesis: comparison with the similar role of chromogranin A, *J. Biol. Chem. 278*, 40581−40589.
72. Lee, J. C., Taylor, C. V., Gaucher, S. P., Toneff, T., Taupenot, L., Yasothornsrikul, S., Mahata, S. K., Sei, C., Parmer, R. J., Neveu, J. M., et al. (2003) Primary sequence characterization of catestatin intermediates and peptides defines proteolytic cleavage sites utilized for converting chromogranin a into active catestatin secreted from neuroendocrine chromaffin cells, *Biochemistry 42*, 6938−6946.
73. Palm, T., Greenfield, N. J., and Hitchcock-DeGregori, S. E. (2003) Tropomyosin ends determine the stability and functionality of overlap and troponin T complexes, *Biophys. J. 84*, 3181−3189.
74. Schaffer, A. A., Aravind, L., Madden, T. L., Shavirin, S., Spouge, J. L., Wolf, Y. I., Koonin, E. V., and Altschul, S. F. (2001) Improving the accuracy of PSI-BLAST protein database searches with composition-based statistics and other refinements, *Nucleic Acids Res. 29*, 2994−3005.

BI700704R